

Supporting Information

Risselada and Marrink 10.1073/pnas.0807527105

SI Methods

This supplementary material contains details about the MARTINI model used in our simulations and details of the method of analysis. Fig. S1 quantifies the different lateral diffusion rates of the 2 cholesterol populations of the L_d phase. Fig. S2 provides additional illustrations of the structure of the L_o/L_d phase coexistence in various lipid mixtures.

The MARTINI Model. All systems were simulated using the MARTINI CG force field (1), version 2.0. The MARTINI model uses a 4-to-1 mapping, i.e., on average 4 heavy atoms are represented by a single interaction center, with an exception for ring-like molecules such as cholesterol that are mapped with somewhat higher resolution (\approx 3-to-1).

The model considers 4 main types of interaction sites: polar (P), intermediately polar (N), apolar (C), and charged (Q). Within a main type, subtypes are distinguished either by a letter denoting the hydrogen bonding capabilities (*d*, donor; *a*, acceptor; *da*, both; \emptyset , none), or by a number indicating the degree of polarity [from 1 (low polarity) to 5 (high polarity)]. In the CG representation, the PC head group consists of 2 hydrophilic groups: the choline (type Q_0) and the phosphate (Q_a) group. The former bears a positive charge, the latter a negative charge. Two sites of intermediate hydrophilicity (N_a) are used to represent the glycerol ester moiety. Palmitoyl tails (C_{16}) are modeled by 4 C_1 particles, and linoleyl tails ($C_{18:2}$) also by 4 particles, the middle 2 by the C_4 type to reflect the more hydrophilic nature of the unsaturated bonds. The other 2 tail beads for the linoleyl tails are of type C_1 . The central location of the C_4 particles in the tail mimics those present in ω_6 fatty acids. Although the resolution of the CG model is necessarily limited, the closest analogue would be *cis,cis*-9,12-octadecadienoic acid (also known as linoleic acid). Cholesterol is represented by 8 CG particles. The hydrophilic head group is modeled as SP_1 (where the S denotes the special ring type), the sterol body by 4 SC_1 and 1 SC_3 particle accounting for the presence of a double bond, and 2 tail particles (SC_1 attached to the sterol body, and C_1 for the terminal group). The solvent is modeled as a single, type P_4 site, each bead representing 4 water molecules.

Nonbonded interactions are described by a Lennard–Jones (LJ) potential. The strength of the pair interaction, determined by the value of the well depth of the LJ potential, depends on the interacting particle types. The full interaction matrix can be found in the original publication (1). In addition to the LJ interaction, the charged lipid head group sites interact via a Coulombic energy function with a relative dielectric constant $\epsilon_{rel} = 15$ for explicit screening. Standard bonded parameters were used for the lipids as well as for cholesterol; details can be found elsewhere (1). Parameters for polyunsaturated chains were not available, and have been optimized using all-atom simulations of Feller *et al.* (2). From quantum mechanical calculations these authors concluded that polyunsaturated chains show an unusually high degree of conformational flexibility compared to mono-unsaturated or saturated chains. To mimic this behavior in the CG model, both the force constant K and the equilibrium angle θ of the angle potential for the CG particles representing the polyunsaturated part of the lipid tails were reduced from the standard values of $K = 45 \text{ kJ mol}^{-1}$ to 10 kJ mol^{-1} and $\theta = 120^\circ$ to 100° . These parameters were further tested by comparing the effective angle distributions obtained from simulations of bulk polyunsaturated alkanes, both at the CG and all-atom level. In addition we compared the level of

backfolding (i.e., the tendency of the lipid tail ends to reside near the interface) in lipid bilayers at both levels of resolution. The characteristic significant increase in backfolding of polyunsaturated lipids is well reproduced at the CG level. The same parameters were recently used to study the interaction of cholesterol and diC_{20:4}-PC (diarachidonoyl-PC), another ω_6 fatty-acid-containing lipid (3). In this study, the characteristic feature of the experimental neutron scattering profiles, namely an increased presence of the cholesterol head group in between the bilayer leaflets, could be reproduced.

Analysis of Structural Properties. Local properties of the lamellar membrane system were computed by dividing the membrane into slabs of 1 nm width in the direction perpendicular to the domain boundaries. Averages were taken over the final 4 μs of the simulation. The local membrane thickness was defined as the average distance between the phosphate groups of both monolayer leaflets in a particular slab. The local area per lipid is calculated as the average amount of lipids (including cholesterol) in a slab divided by the area of that slab. The order parameter represents the segmental order parameter averaged over all 4 tail segments, and all lipid tails present in a particular slab. The local composition of a certain component was defined as the mol fraction of the total amount of components in that slab. The radial distribution function of cholesterol (Fig. 3B) was obtained by considering the distribution of the cholesterol center-of-masses for each of the monolayers separately. All visual images (Figs. 1, 2A, 3A, and 4A and Fig. S2) were prepared using the VMD (Visual Molecular Dynamics) software (4), version 1.8.6.

Analysis of Dynamic Properties. The local lateral diffusion constant was calculated from the average lateral mean square displacement (MSD) of a representative bead in the head group region of the molecule (the phosphate group was chosen for the PC lipids and the hydroxyl group in case of cholesterol) in a slab. All motions were corrected for the overall center of mass motion of the monolayers. Because of the nonlocal nature of the diffusion process, only short time mobilities were taken into account ($t < 4 \text{ ns}$) to prevent dominant contributions to the diffusion rate outside the target slab. Distinction between the 2 cholesterol populations in the L_d phase was based on the position of the cholesterol head group with respect to the membrane normal, assigned to 4 separate bins (2 for the interfaces and 2 for the membrane interior). The average monolayer residence time of cholesterol, or flip-flop time, was estimated by counting the number of crossings. A crossing was defined as a tilt angle changing from a value $\theta > 120^\circ$ to a value $\theta < 60^\circ$ or vice versa. The tilt angle of cholesterol was defined as the angle between the bilayer normal, and the vector connecting the head group site to the tail site that is directly attached to the sterol body. To remove fast reorientations not necessarily indicating a flip-flop, the time series were filtered by applying a running average over 10 ns before counting the number of flip-flop events. For the determination of the exchange ratios of lipids between the domains, 2 small 1 nm wide slabs were defined in the middle of both the L_o and L_d phase, based on the plateaus in the composition profiles (Fig. 2B). An exchange event was counted when a molecule at time $t = \theta$ appeared in the marked region of the L_d phase and at time $t + \Delta t$ ($0 < \Delta t < 4 \mu\text{s}$) in the marked region of the L_o phase or visa versa. The exchange rate per unit length is then defined as the total amount of exchange events observed, divided by the time window of the analyzed trajectory and the

dimension of the simulation box in the direction along the domain interface. The values reported in the main manuscript are averaged over the exchange rates in the 2 directions.

Analysis of Domain Area and Perimeter. To compute the domain area and perimeter of the L_o phase, the following procedure was used to identify the L_o phase. The phosphate beads of diC₁₆-PC in either one of the 2 monolayers were projected on top of a 2D grid with a grid size of 0.5×0.5 nm. Each grid point falling within a radius of 0.4 nm of the projected bead was marked as a domain element. A cluster algorithm based on the direct edge contact between 2 domain grid elements was used to subsequently identify the connectivity of the system. The L_o phase is defined as being the biggest cluster of connected grid elements. A perimeter element is defined as each element of the cluster which has <4 neighbors belonging to the same cluster. The criteria used in this algorithm such as the grid size and the radius of the overlap circle were optimized empirically by overlapping the identified L_o domain with the real structure. The area of the L_o domain is defined as the total number of grid elements multiplied by the area of a grid element. The perimeter/area ratio (Fig. 4C) is defined as the number of perimeter grid elements divided by the total number of grid elements in the L_o domain. The overlap is determined by counting the number of corresponding grid elements of the L_o domain in each monolayer. The overlap fraction is defined as the total number of corresponding grid elements divided by the average number of grid elements of the 2 L_o domains. At the start of the simulation, the overlap fraction is 0.75, corresponding to the expectation value for completely uncoupled monolayer leaflets. The final overlap fraction is close to 0.85. The clustering procedure was also used to identify the cholesterol cluster size distribution (Fig. 3B, *Inset*). The random distribution, used for comparison, was obtained from a simulation of a 2D hard sphere fluid with an overall density equivalent to that of cholesterol in the raft phase.

Analysis of Line Tension. The domain line tension was estimated from the shape fluctuations of the perimeter of the L_o phase (Figs. 4 A and B). From the work of Esposito *et al.* (5), it was shown that the line tension σ for a stable domain can be estimated as $\sigma = 3kTR_0/4\pi \langle (\Delta r_y)^2 \rangle$, with $\Delta r_y = r_y - \langle r_y \rangle$ and $R_0 = \frac{1}{2}A/L_x$. Here r_y denotes the distance between a point on the perimeter and the center of the L_o domain measured along the direction perpendicular to the domain interface. The brackets represent an average over all perimeter points. A is the average area of the domain, and L_x the simulation box length in the direction along the domain boundary. Because we calculated the fluctuations of the perimeter for each of the 2 monolayers independently, the line tension obtained by this method as reported in the main manuscript is the line tension for a single

monolayer. An independent measure of the line tension was obtained from the pressure difference between the 2 lateral membrane directions (6). For a percolating domain along the x direction, the line tension is given by $\sigma = \frac{1}{2}L_x L_z (P_b - P_{yy})$ where $P_b = P_{xx} = P_{zz}$ denotes the pressure in the bulk water and P_{yy} is the pressure tensor component along the domain interface. Assuming independent fluctuations of the domains in both monolayers, the line tension per monolayer interface is 0.5σ . Both estimates of the line tension were found to be equivalent within the statistical error.

Analysis of Monolayer–Monolayer Surface Tension. The surface tension driving the L_o domain–domain coupling was estimated from the probability distribution $P(\Delta A)$ of the mismatch area $\Delta A = (1 - \alpha)A_0$ between the 2 domains, with α denoting the overlap fraction (see *Analysis of Domain Area and Perimeter*, above) and $A_0 (= 313 \text{ nm}^2)$ the equilibrium L_o domain area. The histogram was constructed from the fluctuations in the area overlap fraction over the last 10 μs of the simulation (after macroscopic phase separation had occurred). The resolution for distinction of 2 nearest states was chosen to be 0.01 overlap fraction. Assuming that, for large mismatch areas, the dominant contribution to the free energy of the system arises from the surface tension γ between the L_o and L_d phases, we can write $P(\Delta A) \sim e^{-\gamma\Delta A}$. Fitting $\ln P$ in the regime of a large mismatch area (Fig. 4D) gives a surface tension $\gamma = 0.15 \pm 0.05 \text{ kT nm}^{-2}$.

Error Estimates. The statistical error in the structural and dynamic properties presented in the main manuscript was assessed by using a block averaging procedure, considering blocks of 500 ns as independent. The last 4 μs were used for the analysis. Together with the separation of the results for both monolayers, 16 measures were obtained on which the standard error estimate was based. Statistical errors in the case of the composition, the order parameters, the area/lipid, and the thickness are small, comparable to the size of the symbols in Fig. 2 B and C. In the calculation of the local lateral lipid diffusion constants the nonlocal nature of the diffusive process introduces a systematic error. The size of this error (displayed in Fig. 2D) was estimated from the spread of values obtained within a specific slab. For the flip-flop rate no accurate error bars could be derived, especially toward and inside the L_o phase, because of the limited number of events observed. The flip-flop profile in Fig. 2D is therefore of more qualitative nature. The error estimates for the line and surface tensions are also based on a division of the simulation trajectory, in this case by using somewhat larger block lengths of 1 μs . The choice of the exact resolution with which the raft-like phase and perimeter were characterized proved insignificant compared to the spread in values obtained for the individual blocks.

1. Marrink SJ, Risselada HJ, Yefimov S, Tieleman DP, de Vries AH (2007) The MARTINI force field: Coarse grained model for biomolecular simulations *J Phys Chem B* 111:7812–7824.
2. Feller SE, Gawrisch K, MacKerell AD, Jr (2002) Polyunsaturated fatty acids in lipid bilayers: Intrinsic and environmental contributions to their unique physical properties *J Am Chem Soc* 124:318–326.
3. Marrink SJ, de Vries AH, Harroun TA, Katsaras J, Wassall SR (2008) Cholesterol shows preference for the interior of polyunsaturated lipid. *J Am Chem Soc* 130:10–11.

4. Humphrey W, Dalke A, Schulten K (1996) VMD - Visual Molecular Dynamics. *J Mol Graphics* 14:33–38.
5. Esposito C, *et al.* (2007) Flicker spectroscopy of thermal lipid bilayer domain boundary fluctuations. *Biophys J* 93:3169–3181.
6. Tolpekina TV, den Otter WK, Briels WJ (2004) Simulations of stable pores in membranes: System size dependence and line tension. *J Chem Phys* 121:8014–8020.

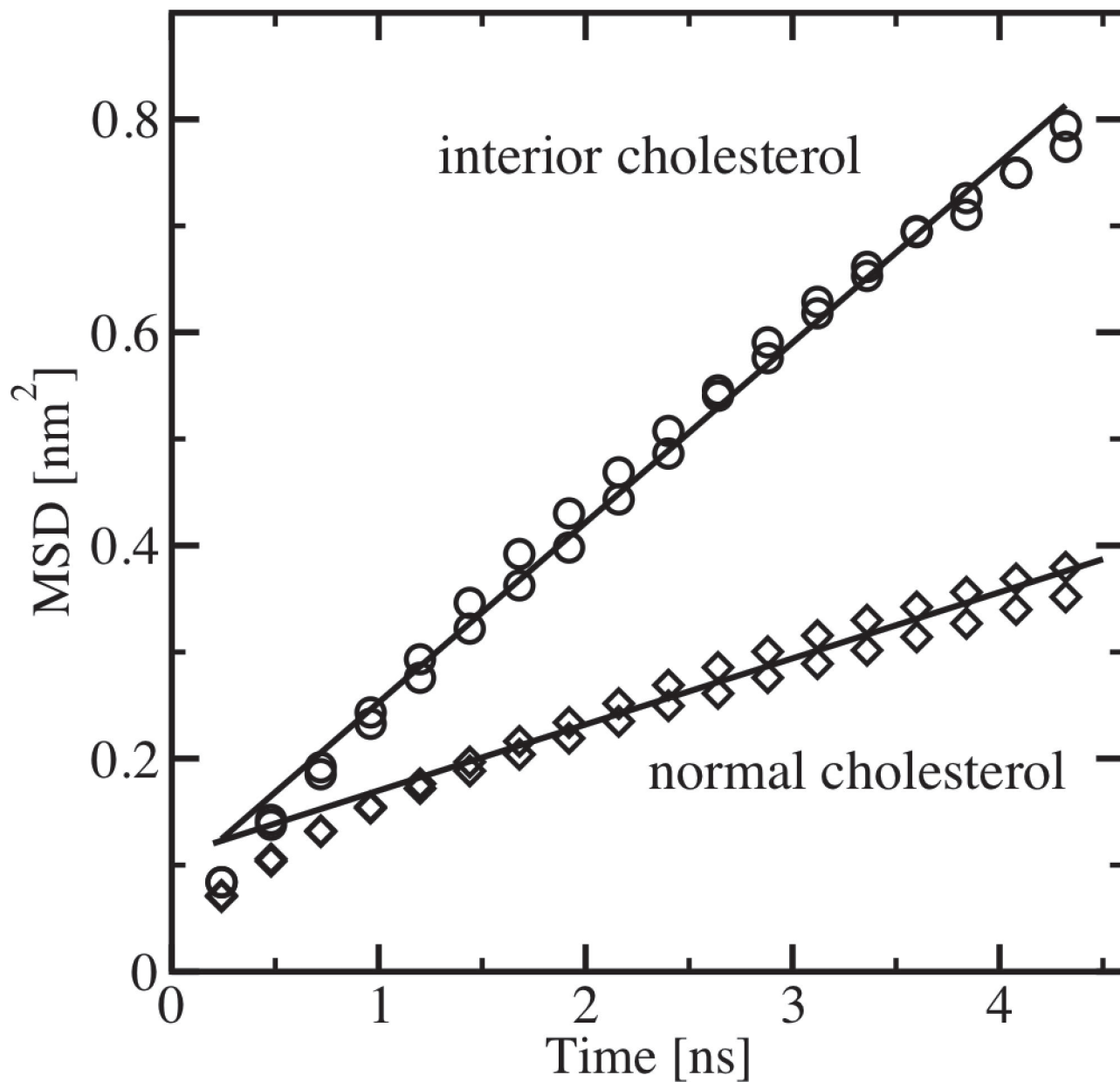


Fig. S1. Two cholesterol populations in L_d phase differ in lateral mobility. The lateral mean squared displacement (MSD) of cholesterol molecules in the L_d phase is shown as a function of time, separated into the contribution from cholesterol molecules embedded in between the monolayer leaflets ("interior") and cholesterol molecules oriented with their headgroup near the interface ("normal"). From the slope of the MSD curves (solid lines), the lateral diffusion coefficient is found to be $D_{\text{interior}} = 41 \pm 3 \times 10^{-8} \text{ cm}^2\text{s}^{-1}$ for the interior population, and $D_{\text{normal}} = 14 \pm 1 \times 10^{-8} \text{ cm}^2\text{s}^{-1}$ for the normal population. The average rate is $D_{\text{total}} = 20 \pm 1 \times 10^{-8} \text{ cm}^2\text{s}^{-1}$, dominated by the larger fraction of the normal population (normal:interior \approx 4:1). The value of D_{normal} is close to that obtained for the diC_{18:2}-PC lipids in the L_d phase (compare Fig. 2D), implying that the faster average mobility of cholesterol is because of the small interior population. The circles and diamonds indicate individual data points for the interior and normal cholesterol populations, separated into 2 sets arising from the 2 interfacial slabs (normal) or 2 interior slabs (interior) that were used for the analysis.

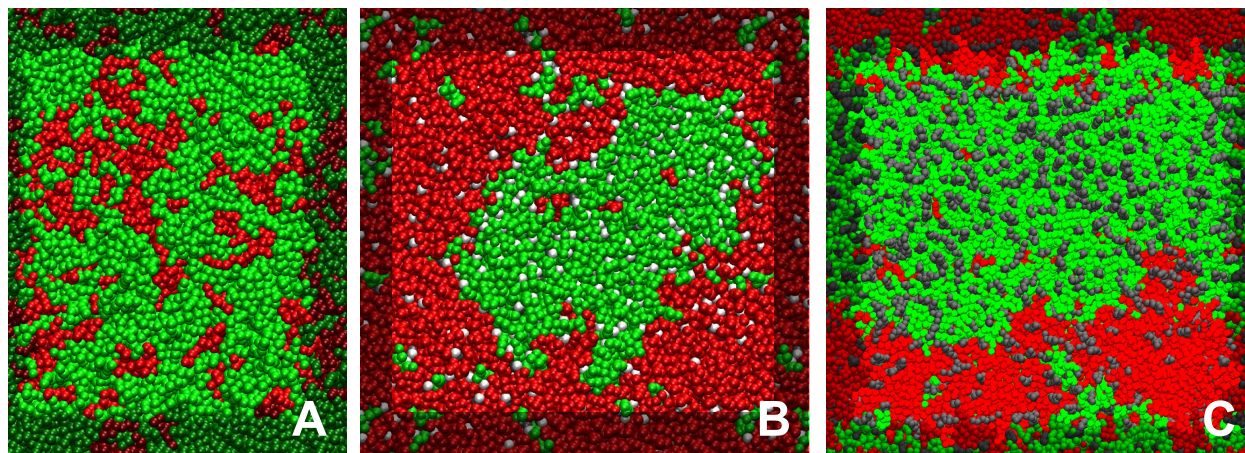


Fig. S2. Cholesterol is required to induce formation of large domains. (A) A binary diC₁₆-PC/diC_{18.2}-PC 3:1 mixture shows no domain formation, although the mixing is nonrandom. The domain sizes are similar to those present in the ternary mixture 1 μ s after the quench (see Fig. 1B). Note that both domains remain in the fluid phase at $T = 295$ K (H.J.R. and S.J.M., unpublished work). (B and C) Complete phase separation is observed in the diC₁₆-PC/diC_{18.2}-PC/cholesterol 0.28:0.42:0.3 (B) and 0.42:0.28:0.3 (C) ternary mixtures at $T = 295$ K. Green is used for the saturated lipids and red for the polyunsaturated lipids. Cholesterol is depicted in gray with a white (B) or gray (C) hydroxyl group.